Global distribution of reversed energy spectra of ring current protons based on Van Allen Probes observations

Juan Yi[1], Song Fu[1*], Binbin Ni[1,2*], Xudong Gu[1], Man Hua[1], Zheng Xiang[1], Xing Cao[1], Run Shi[1], and Yiwen Zhao[1]

[1] Department of Space Physics, School of Electronic Information, Wuhan University, Wuhan, China

[2] CAS Center for Excellence in Comparative Planetology, Hefei, China

Corresponding authors: Drs. Song Fu and Binbin Ni, Wuhan University

Email: fusion@whu.edu.cn, bbni@whu.edu.cn

Key Points:

- The reversed energy spectra of ring current protons were observed by RBSPICE to show the distinct flux minima ~50 - 100 keV and flux maxima ~200 - 400 keV.
- The reversed proton energy spectra mostly occur inside the plasmasphere during geomagnetically quiet periods.
- The global distributions of reversed proton energy spectra suggest the underlying contributions of various physical processes.

Abstract

Energy spectra of ring current protons are crucial to understanding the ring current dynamics. Based on high-quality Van Allen Probes RBSPICE measurements, we investigate the global distribution of the reversed proton energy spectra using the 2013-2016 RBSPICE datasets. The reversed proton energy spectra are characterized by the distinct flux minima around 50 - 100 keV and flux maxima around 200 - 400 keV. Our results show that the reversed proton energy spectrum is prevalent inside the plasmasphere, with the occurrence rates > 90% at L ~ 2 - 4 during geomagnetically quiet periods. Its occurrence also manifests a significant decrease trend with increasing L-shell and enhanced geomagnetic activity. It is indicated that the substorm-associated processes are likely to lead to the disappearances of the reversed spectra. These results provide important clues for exploring the underlying physical mechanisms responsible for the formation and evolution of reversed proton energy spectra.

Plain language summary

The energy spectra of ring current protons are significant for us to understand the ring current dynamics. Several previous studies reported the reversed energy spectra of ring current protons that represent flux minima at lower energies and flux maxima at higher energies. In the literature, there is rather limited statistical investigation on the global distribution features of such spectra. The availability of high quality Van Allen Probes RBSPICE data enables a comprehensive study in this regard. Based on RBSPICE measurements, we report the reversed energy spectra of ring current protons particularly featured by the distinct flux minima around 50 - 100 keV and flux maxima around 200 - 400 keV. We further adopt 4-year RBSPICE proton datasets from 2013 to 2016 to investigate the occurrence rate, corresponding energies of flux maximum and minimum, and the ratio of flux maximum to minimum as a function of

L shell, MLT and geomagnetic activity level. Our results demonstrate that these reversed proton energy spectra are prevalent inside the plasmasphere, with the occurrence rates > 90% at L ~ 2 – 4 during geomagnetically quiet periods. The strong L and geomagnetic activity dependence imply the physical processes in association with proton substorm injections.

1. Introduction

Energy spectrum distributions of energetic particles are an essential indicator for understanding the underlying physics of magnetospheric particle dynamics. In general, it is well recognized that both electron and proton energy spectra in space plasmas follow a Kappa or Kappa-like profile having fluxes steeply falling with increasing energy (e.g., Freden, 1965; Pizzella et al., 1962; Summers et al., 2009). In contrast, a number of previous studies reported 'reversed' energy spectra of energetic particles that do not follow monotonically decrease profiles of fluxes with increasing energy but represent flux minima at lower energies and flux maxima at higher energies. Based on the Molniya 1 measurements, Vakulov et al. (1975) observed a flux maximum of the outer belt electron energy spectra at energy ~1- 2 MeV. West et al. (1981), using 60 keV to 3 MeV electron data from Ogo5, showed a flux maximum at ~1.5 MeV and a minimum at ~500 keV. By analyzing the ring current proton spectra (1 - 300 keV) observed by the Explorer 45, Williams et al. (1973) reported the flux minima of proton energy spectra at energies ~20 - 100 keV over L ~ 3.2 - 4.0, which they attributed to the ion-cyclotron instability. Based on the AMPET CCE measurements, Krimigis et al. (1985) observed the flux maxima at energies ~100 - 300 keV during both the main and recovery phases of a geomagnetic storm.

Along with the launch of the twin Van Allen Probes mission in August 2012 (Mauk et al., 2012), the long-term accumulation of unprecedented, high quality particle datasets with fine energy resolutions has fueled a resurgence in magnetospheric particle dynamics studies. By combining the MagEIS and REPT

measurements, Zhao et al. (2019a) reported a reversed energy spectrum of radiation belt electrons, which is featured by the flux maximum ~1 – 2 MeV and flux minimum ~ 100's keV and is reasonably accounted for energy-dependent electron losses induced by hiss wave (e.g., Ni et al., 2019; Fu et al., 2020). A following statistical analysis of Zhao et al. (2019b), on basis of the detailed analysis of reversed electron energy spectra, found that reversed energy spectra dominate inside the plasmasphere at $L < 2.5$.

Comparatively, there remains lacking the systematic information about the global distribution of the reversed energy spectra of ring current protons. The availability of Van Allen Probes RBSPICE data enables a comprehensive study in this regard. Therefore, this letter is dedicated to investigate the global distribution of reversed proton energy spectra based upon multi-year RBSPICE data from Van Allen Probes. By establishing an automatic identification criterion for the reversed proton energy spectra, we intend to perform a statistical analysis to explore the global distribution features of the reversed proton energy spectrum, its occurrence pattern, its dependence on geomagnetic activity, and its profile characteristics in terms of the energy range of local flux minimum and the ratio of local flux maximum to minimum.

2. Instrumentation and Datasets

The Van Allen Probes, launched in August 2012, consist of two identical satellites and operate in almost same orbits with perigees of ~600 km, inclination of ~10°, apogees of ~5.8 Earth radii (R_E) and spin period of ~11s (Mauk et al., 2012). The Radiation Belt Storm Probes Ion Composition Experiment (RBSPICE) instrument onboard the Van Allen Probes, which are designed to obtain a comprehensive physical understanding of ring current, provides measurements of protons in the energy range of ~7 - 600 keV (Mitchell et al., 2013). The level 3-PAP data with pitch angle information are adopted in this study. Due to the high-voltage issues during the early phase of the emission of RBSPICE-A, we only adopted the data from RBSPICE-B in the present study (Summers et al., 2017). The L shell used

in this study is McIlwain L calculated with IGRF and OP77Q (Olson and Pfitzer, 1982) magnetic field model.

3. Observations and Statistical Results

Figure 1 displays the observations of proton fluxes during 16 - 30 March, 2015. The solar wind parameters and geomagnetic indices obtained from the OMNIweb are plotted in Figures 1a-b. On 17 March 2015 when an intense geomagnetic storm occurred, the solar wind speed jumped from ~400 to ~600 km/s and the interplanetary magnetic field (IMF) B_z turned quickly from northward (~15 nT) to southward (~-15 nT). The Dst index dropped from ~30 to ~-220 nT with the AE index increasing significantly from ~100 to 1500 nT. At the same time, the RBSPICE onboard the Van Allen Probe B observed evident proton flux increases at energies of 44.7 and 81.6 keV (Figures 1c-d). However, the enhancements of 268.9 keV proton fluxes did not occur until 18 March. The black solid lines in Figures 1c-e indicate the plasmapause location calculated using Liu et al., (2015) model. In Figures 1c-d, the proton fluxes outside the plasmasphere are higher than those inside the plasmasphere during quiet times. During the recovery phase after 18 March, 44.7 and 81.6 keV proton fluxes at lower L (~2 – 4) gradually decreased while the 268.9 keV proton fluxes increased and then remained relatively stable. Figures 1f-h further show the proton energy spectra at the indicated time intervals. As shown in Figure 1f, the proton fluxes generally decreased monotonically with increasing energy over L ~3.0 – 5.6. However, several days later (Figures 1g-h), the proton energy spectra at L < ~5.2 exhibited “reversed” structures with fluxes decay more significantly at low energies < ~200 keV, leading to flux minima at energies ~80 keV. These flux minima reduced with decreasing L shells.

Figure 2 illustrates some key parameters of the reversed proton energy spectra. This representative example occurred at 02:04:47 on 29 March 2015at L = 3.15. In this example, proton energy spectrum has a clear flux minimum (f_{min}) at E_{min} ~82 keV and a flux maximum (f_{max}) at E_{max} ~221 keV with the ratio of flux maximum to

minimum reaching ~60. To automatically identify the reversed proton energy spectra, we adopted three criteria: (1) proton energy spectra show the existence of the maximum and minimum, and the corresponding energy of flux maximum (E_{max}) is greater than that of flux minimum (E_{min}), (2) $\frac{f_{max}}{f_{min}} > 3$, and (3) there must be at least one energy channel between the E_{max} and E_{min} to avoid the misclassification.

To further investigate the relation between the geomagnetic activities and the reversed proton spectra in a long period, we present the geomagnetic indices and proton fluxes with three energy channels (44.7, 81.6 and 268.9 keV) during 2015 in Figures 3a-d with the white solid lines representing plasmapause locations. When the Dst index suddenly decreased and the AE index increased, the locations of plasmapause were reduced to lower L (~2 – 3). For 44.7 and 81.6 keV protons, the fluxes outside the plasmasphere are ~1 order of the magnitude higher than those inside the plasmasphere in most cases, yet this is opposite to the fluxes of 268.9 keV protons. While inside the plasmasphere, the proton fluxes at energies 44.7 and 268.9 keV are generally 1~2 orders higher than those at energies 81.6 keV. With increasing energy, the proton energy spectra are going to show the decreasing and then increasing trend which is the reversed feature depicted in Figure 2. Figures 3e-h demonstrate the key parameters of automatically selected reversed proton energy spectra. The occurrence rate of the reversed proton energy spectra is calculated with the grids of 0.1 L and one day. The locations of plasmapauses match well with the upper boundaries of the region with the occurrence rate > 90%. During quiet times, the plasmapauses usually locate at L > 4.5 so that the reversed proton energy spectra locate at L ~2 – 4. We find that the proton reversed energy spectra are likely to be observed under active geomagnetic conditions (Dst > -50 nT and the AE > 1000 nT). As shown in Figures 3f-h, the proton energies of flux maxima mostly lie in the range of ~82-400 keV, decreasing with increasing L shells. Similarly, the proton energies of flux minima for reversed energy spectra are tens of keV. Note that there still are a few

events which distribute outside the plasmasphere at L > ~4.5 with E_{max} > 328 keV and E_{min} > 100 keV. Figure 3f reveals that the flux maxima are ~10 to 30 times greater than the flux minima at L < 4, while the ratios decrease from ~10 to 3 with increasing L shells at L > 4.

Figure 4 shows the global distributions of reversed proton energy spectra as a function of L shell and MLT for three indicated geomagnetic conditions (Dst>-30 nT, -50 nT<Dst<-30 nT and Dst<-50 nT) from January 2013 to December 2016. From top to bottom, each row presents the number of total samples, occurrence rate, the corresponding energies of flux maximum and minimum, and the ratio of flux maximum to minimum. The region of our interest has been divided into smaller bins with the resolution of 0.5 L × 1 MLT, and the blank bins means the observational samples are less than 50. Both the E_{max}, E_{min}, and the ratio of flux maximum to minimum in Figures 4g-o are valued by averaging the cases in one bin. Most samples are observed during quiet times (Dst > -30 nT) at L ~2.5 - 4.5 (Figure 4a). The reversed proton spectra almost persistently exist over L ~ 2 – 4 during quiet times, with occurrence rates >90%. Besides, the occurrence rates decrease with increasing L shells, which is consistent with the observations shown in Figure 1, and decreases under more active geomagnetic activities. The upper boundary of higher occurrence rate (>90%) regions shift from higher to lower L shells. Regarding to the MLT dependence, we find that the occurrence rates on the dayside are slightly higher than those of nightside, especially during the geomagnetically active periods (Dst < -50 nT). In Figures 4g-l, the statistical distributions of the E_{max} and E_{min} demonstrate that the proton fluxes mostly reach the peaks at energies ~200 - 400 keV and drop to the valleys at energies ~50 - 100 keV. Both E_{max} and E_{min} decrease first as the L shell increases to ~5, while they suddenly increase on two MLT sectors (15-19, 22-05) at L>5 with relatively small samples. In addition, the statistics of E_{max} and E_{min} show a less geomagnetic activity dependence. The ratios decrease with the increasing L shells, which are smaller under the more active geomagnetic conditions (Figures 4m-o).

4. Discussions

Our results show that the reversed proton spectra are preferentially inside the plasmasphere and show significant losses of lower energy (~50 - 100 keV) protons after the geomagnetic storm (Figures 1f-h). It is significant for us to further understand the mechanisms that produce the reversed proton energy spectra. There are several possible explanations for the formation of the reversed proton energy spectra.

Firstly, charge exchange is found to be the main loss process of ring current protons by capturing electrons from neutral atoms (Ebihara & Ejiri, 2003; Dessler & Parker, 1959; Smith & Bewtra, 1976). The lifetime of proton due to charge exchange is shortest at energies around tens of keV with the value of 0.2 – 1 day (Fok et al., 1991). This energy range is consistent with our statistical distributions of E_{min} in reversed proton spectra. Furthermore, the densities of neutral hydrogen are higher at lower L shells (Østgaard et al., 2003). Thus, the loss effect due to charge exchange is stronger at lower L shells. We also find that the reversed proton energy spectra show a high occurrence at low L shells (L=2 - 4). These agreements in spatial distribution suggest that charge exchange plays an important role in the formation of reversed proton energy spectral.

Another candidate for the loss of protons is Coulomb collision (Fok et al., 1996; Jordanova et al., 1996, 1999). When particles travel through the plasma, they will loss energy or change pitch angles due to collisions with other particles. Similar to charge exchange, Coulomb collision also likes to occur in lower L shells (Fok et al., 1991). However, this process is dominant in decreasing the proton fluxes at low-energies (<10 keV) (Fok et al., 1996) and is not likely to produce the reversed proton energy spectra with local minima at energies ~50 - 100 keV.

There are also two collisionless scattering mechanisms for the ring current decay: wave-particle interactions and field line curvature (FLC) scattering. The electromagnetic ion cyclotron (EMIC) waves can effectively scatter several keV to hundreds of keV protons into the loss cone due to pitch angle diffusion with a time

scale of a few hours (Cao et al., 2019, 2020; Cornwall, 1977; Jordanova et al., 1997; Xiao et al., 2011; Summers, 2005). The field line curvature scattering is of importance for the ring current decay when the field line configuration is stretching (Chen et al., 2019; Ebihara et al., 2011; Sergeev et al., 1993; Yu et al., 2020). Yu et al. (2020) investigated the role of FLC scattering in ring current decay during the 17 March 2013 storm and found that the associated proton precipitation mainly occurs at $L > 5$ on the nightside. This finding is basically consistent with our observations that the reversed proton energy spectra are distributed at $L > 5$ on two MLT sectors (15-19, 22-05). The formation mechanism of reversed energy spectra at $L>5$ may be different from those at $L<5$.

Although several loss mechanisms have been proposed to explain the decay of Earth's ring current. The relative contributions of difference mechanisms to the formation of the reversed proton energy spectra still remain to be fully understood, which however is outside the scope of this study and is left to a future study.

5. Conclusions

In this study, based on the high-resolution proton flux data from RBSPICE onboard the Van Allen Probe B during 2013 – 2016, we have performed a detailed statistical analysis of the global distribution of reversed energy spectra of ring current protons. The major conclusions are summarized as follows:

(1) The reversed proton energy spectra are preferentially observed inside the plasmasphere, with the occurrence rates > 90% at $L \sim 2$ - 4 during geomagnetically quiet periods. As the geomagnetic activity intensifies, the preferential occurrence region of the reversed proton energy spectra shrinks to lower L shells (~2.5 - 3.5).

(2) The proton energies corresponding to the flux maxima and minima of the reversed energy spectra decrease with the increase of L shell in the region of $L < 5$. The flux minima of the reversed proton spectra mainly occur at ~50 - 100 keV, while the flux maxima are generally present at ~200 - 400 keV.

(3) Similar to the global distribution of the reversed spectrum occurrence rate,

the ratios between flux maxima and minima are strongly L shell and geomagnetic activity dependent, showing that the ratios during active times and at higher L shells are smaller than those during quiet times and at lower L shells.

Acknowledgments

This work was supported by the National Natural Science Foundation of China (grant nos. 42025404, 41674163, 41704162, 41974186, 41674162, 41904144, 41904143), the B-type Strategic Priority Program of the Chinese Academy of Sciences (grant no. XDB41000000), the pre-research projects on Civil Aerospace Technologies (grant nos. D020303, D020308, D020104) funded by the China National Space Administration, the National Key R&D Program of China (2018YFC1407303) and the China Postdoctoral Science Foundation Project (grant no. 2019M662700). We also acknowledge the Van Allen Probes mission, particularly the RBSPICE team, for providing particle data. at http://rbspice.ftecs.com. Profiles of the solar wind parameters and geomagnetic indices are from the OMNI website (http://omniweb. gsfc.nasa.gov).

References

Cao, X., Ni, B., Summers, D., Shprits, Y. Y., Gu, X., Fu, S., Lou, Y., Zhang, Y., Ma, X., Zhang, W., Huang, H., & Yi, J. (2019). Sensitivity of EMIC wave‐driven scattering loss of ring current protons to wave normal angle distribution. Geophysical Research Letters, 46, 590–598. https://doi.org/10.1029/2018GL081550

Cao, X., Ni, B., Summers, D., Shprits, Y. Y., & Lou, Y. (2020). Effects of polarization reversal on the pitch angle scattering of radiation belt electrons and ring current protons by EMIC waves. Geophysical Research Letters, 47, e2020GL089718. https://doi.org/10.1029/2020GL089718

Fok, M.-C., Kozyra, J. U., Nagy, A. F., & Cravens, T. E. (1991). Lifetime of ring current particles due to coulomb collisions in the plasmasphere. Journal of

Geophysical Research, 96(A5), 7861– 7867. https://doi.org/10.1029/90JA02620

Fok, M.-C., Moore, T. E., & Greenspan, M. E. (1996). Ring current development during storm main phase. Journal of Geophysical Research, 101(A7), 15,311–15,322. https://doi.org/10.1029/96JA01274

Fu, S., Yi, J., Ni, B., Zhou, R., Hu, Z., Cao, X., et al. (2020). Combined scattering of radiation belt electrons by low frequency hiss: Cyclotron, Landau, and bounce resonances. Geophysical Research Letters, 47, e2020GL086963. https://doi.org/10.1029/2020GL086963

Freden, S. C., Blake, J. B., & Paulikas, G. A. (1965). Spatial variation of the inner zone trapped proton spectrum. Journal of Geophysical Research, 70(13), 3113–3116. https://doi.org/10.1029/JZ070i013p03113

Jordanova, V. K., Kozyra, J., Nagy, A., & Khazanov, G. (1997). Kinetic model of the ring current-atmosphere interactions. Journal of Geophysical Research, 102(A7), 14,279–14,291. https://doi.org/10.1029/96JA03699

Krimigis, S. M., McEntire, R. W., Potemra, T. A., Gloeckler, G., Scarf, F. L., & Shelley, E. G. (1985). Magnetic storm of September 4, 1984—A synthesis of ring current spectra and energy densities measured with AMPTE/CCE. Geophysical Research Letters (ISSN 0094-8276), 12, 329-332. http://doi.org/10.1029/GL012i005p00329

Liu, X., Liu, W., Cao, J. B., Fu, H. S., Yu, J., & Li, X. (2015). Dynamic plasmapause model based on THEMIS measurements. Journal of Geophysical Research: Space Physics, 120, 10,543–10,556. https://doi.org/10.1002/2015JA021801

Mauk, B. H., Fox, N. J., Kanekal, S. G., Kessel, R. L., Sibeck, D. G., & Ukhorskiy, A. (2012). Science objectives and rationale for the Radiation Belt Storm Probes mission. Space Science Reviews, 1–15. https://doi.org/10.1007/s11214-012-9908-y

Mitchell, D. G., Lanzerotti, L. J., Kim, C. K., Stokes, M., Ho, G., Cooper, S., …

Kerem, S. (2013). Radiation belt storm probes ion composition experiment (RBSPICE). Space Science Reviews, 179. https://doi.org/10.1007/s11214-013-9995-4

Ni, B., Huang, H., Zhang, W., Gu, X., Zhao, H., Li, X., Baker, D. N., Fu, S., Xiang, Z., & Cao, X. (2019). Parametric sensitivity of the formation of reversed electron energy spectrum caused by plasmaspheric hiss. Geophysical Research Letters, 46, 4134–4143. https://doi.org/10.1029/2019GL082032

Olson, W. P., & Pfitzer, K. A. (1982). A dynamic model of the magnetospheric magnetic and electric fields for July 29, 1977. Journal of Geophysical Research, 87, 5943–5948. https://doi.org/10.1029/JA087iA08p05943

Ostgaard, N., Mende, S. B., Frey, H. U., Gladstone, G. R., & Lauche, H. (2000). Neutral hydrogen density profiles derived from geocoronal imaging. Journal of Geophysical Research Space Physics, 108, 1300.

Pizzella, G., Laughlin, C. D., & O'Brien, B. J. (1962). Note on the electron energy spectrum in the inner Van Allen Belt. Journal of Geophysical Research, 67(9), 3281–3287. https://doi.org/10.1029/JZ067i009p03281

Summers, D. (2005). Quasi−linear diffusion coefficients for field−aligned electromagnetic waves with applications to the magnetosphere. Journal of Geophysical Research, 110, A08213. https://doi.org/10.1029/2005JA011159

Summers, D., Tang, R., & Thorne, R. M. (2009). Limit on stably trapped particle fluxes in planetary magnetospheres. Journal of Geophysical Research, 114, A10210. https://doi.org/10.1029/2009JA014428

Summers, D., Shi, R., Engebretson, M. J., Oksavik, K., Manweiler, J. W., & Mitchell, D. G. (2017). Energetic proton spectra measured by the Van Allen Probes. Journal of Geophysical Research: Space Physics, 122, 10,129–10,144. https://doi.org/10.1002/2017JA024484

Vakulov, P. V., Kovrygina, L. M., Mineev, I. V., & Tverskaia, L. V. (1975). Dynamics of the outer belt of energetic electrons during moderate magnetic disturbances. Geomagnetizm I Aeronomiia, 15, 1028–1032.

West, H. I. Jr., Buck, R. M., & Davidson, G. T. (1981). The dynamics of energetic

electrons in the Earth's outer radiation belt during 1968 as observed by the Lawrence Livermore National Laboratory's spectrometer on Ogo 5. Journal of Geophysical Research, 86(A4), 2111–2142. https://doi.org/10.1029/JA086iA04p02111

Williams, D. J., Fritz, T. A., & Konradi, A. (1973). Observations of proton spectra (1.0 ≤ Ep ≤ 300 keV) and fluxes at the plasmapause. Journal of Geophysical Research, 78, 4751–4755. https://doi.org/10.1029/JA078i022p04751

Xiao, F., Chen, L., He, Y., Su, Z., & Zheng, H. (2011). Modeling of precipitation loss of ring current protons by electromagnetic ion cyclotron waves. Journal of Atmospheric and Solar - Terrestrial Physics, 73, 106–111. https://doi.org/10.1016/j.jastp.2010.01.007

Zhao, H., Ni, B., Li, X., Baker, D. N., Johnston, W. R., Zhang, W., et al. (2019a). Plasmaspheric hiss waves generate a reversed energy spectrum of radiation belt electrons. Nature Physics, 15(4), 367–372. https://doi.org/10.1038/s41567-018-0391-6

Zhao, H., Johnston, W. R., Baker, D. N., Li, X., Ni, B., Jaynes, A. N., Kanekal, S. G., Blake, J. B., Claudepierre, S. G., Reeves, G. D., & Boyd, A. J. (2019). Characterization and evolution of radiation belt electron energy spectra based on the Van Allen Probes measurements. Journal of Geophysical Research: Space Physics, 124, 4217–4232. https://doi.org/10.1029/2019JA026697

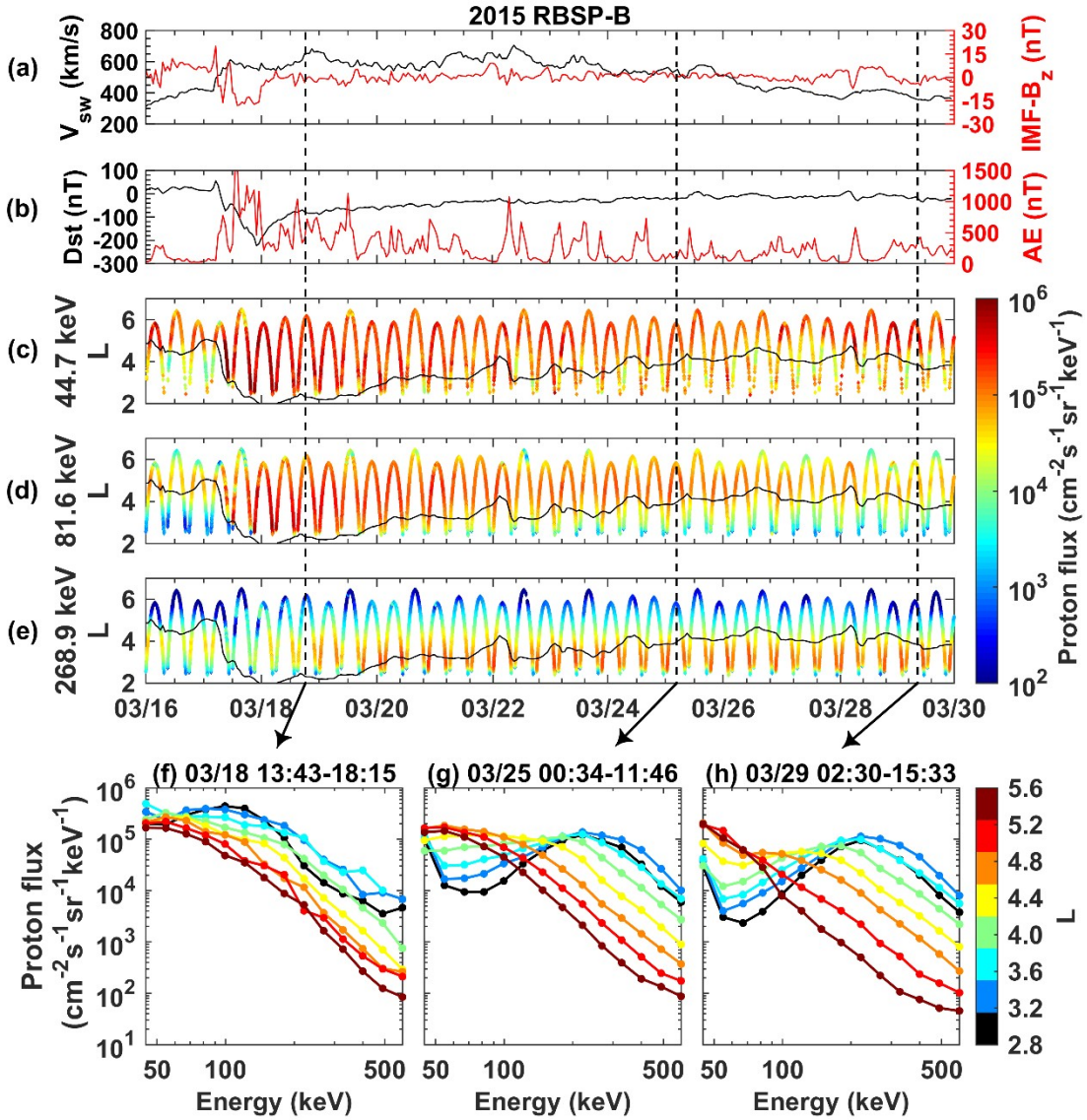

Figure 1. An overview of the 17 March 2015 strong geomagnetic storm. (a) solar wind speed (V_{sw}) and interplanetary magnetic field (IMF) B_z, (b) Dst and AE indices, (c-e) 90° pitch angle proton fluxes at energies of ~44.7 keV, ~81.6 keV, and ~268.9 keV, respectively, with the black solid lines indicating the plasmapause location. (f-h) The proton energy spectra at L ~ 2.8 - 5.6 during three indicated time intervals of the storm.

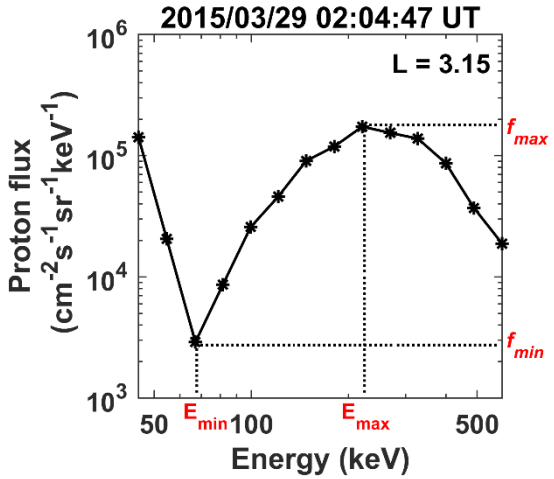

Figure 2. A representative example of the reversed proton energy spectrum at L = 3.15 based on the RBSPICE measurements at 02:04:47 UT on 29 March 2015. Four characteristic parameters of the reversed energy spectrum, i.e., flux maximum (f_{max}), flux minimum(f_{min}), the energy of flux maximum (E_{max}), and the energy of flux minimum (E_{min}), are defined on the plot.

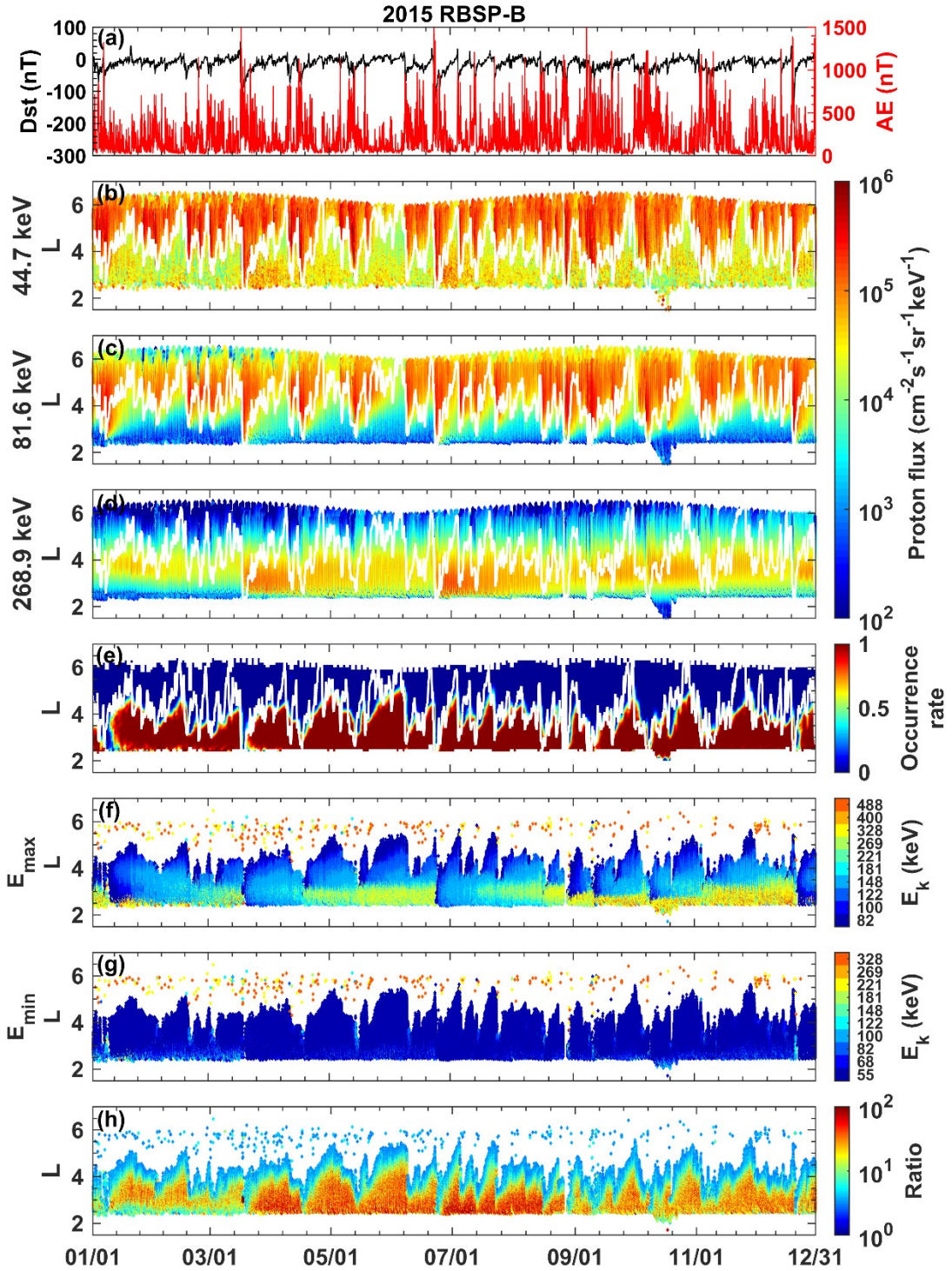

Figure 3. RBSPICE observations of proton fluxes during 2015 and the corresponding distributions of reversed proton energy spectra. (a) Dst and AE indices, (b-d) 90° pitch angle proton fluxes at energies of ~44.7 keV, ~81.6 keV, and ~268.9 keV, respectively, (e) occurrence rate of the reversed proton energy spectrum, (f) the proton energy of flux maximum, (g) the proton energy of flux minimum, and (h) the ratio of proton flux maximum to minimum. The white solid lines in (b-e) indicate the plasmapause location.

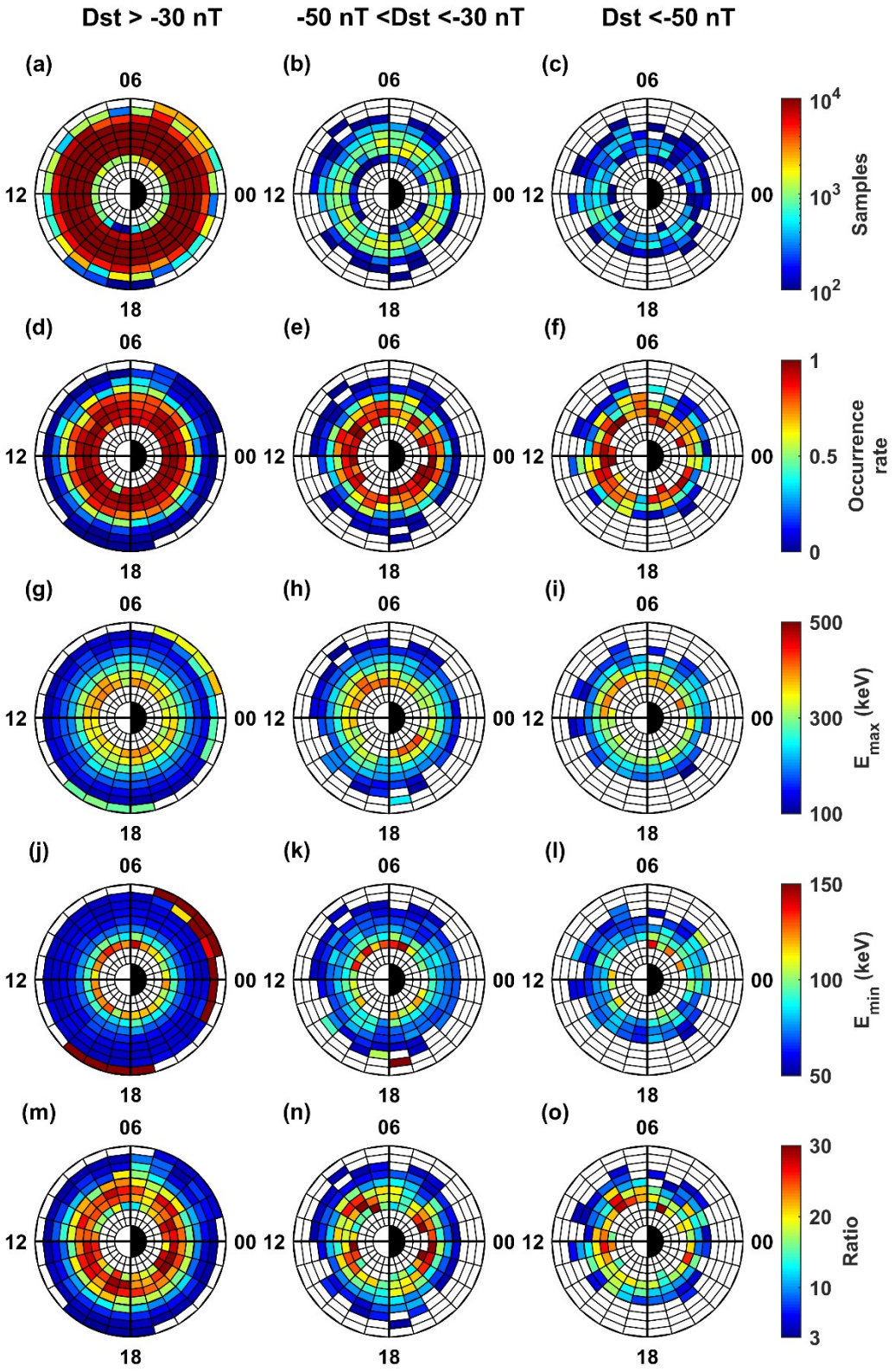

Figure 4. Statistical results of the global distribution of reversed proton energy spectrum during 2013-2016 under the indicated three geomagnetic conditions (from left to right: Dst > -30 nT, -50 nT < Dst < -30 nT, and Dst < -50 nT). (a-c) samples, (d-f) occurrence rate, (g-i) the proton energy of flux maximum, (j-l) the proton energy

392 of flux minimum, and (m-o) the ratio of the proton flux maximum to minimum.